Gain and Bandwidth Enhancement of a Metamaterial Loaded Antipodal Vivaldi Antenna Fed by Substrate Integrated Waveguide

Arman BORDBAR, Farzad MOHAJERI, Zahra GHORBANI

Dept. of Communications and Electronics, School of Electrical and Computer Engineering, Shiraz University, Zand Street, Shiraz, Iran

armanbordbar1990@gmail.com, mohajeri@shirazu.ac.ir, zghorbani2010@gmail.com

Submitted October 25, 2021 / Accepted March 27, 2022

Abstract. *This paper proposes a novel wideband, high-gain, compact Vivaldi antenna operating in the 14.7–20.5 GHz frequency range, where the antenna is fed by the substrate integrated waveguide (SIW). A Negative Index Metamaterial (NIM) has been designed, with its parameters extracted using MATLAB software. The NIM was developed to address the deficiencies of conventional Antipodal Vivaldi antennas. With a measured gain of over 5.3 dBi, the fabricated antenna performs satisfactorily across the entire bandwidth. Due to its low profile and short transversal dimension, the proposed antenna is suitable for antenna arrays; consequently, the proposed antenna design could be a viable option for modern communication and radar systems.*

Keywords

Antipodal Vivaldi, bandwidth, gain, negative index metamaterial, substrate integrated waveguide (SIW)

1. Introduction

Existing wireless systems require ultra-wideband performance, a high bit rate, and increased capacity. Due to its unique characteristics such as relatively wide bandwidth, high efficiency, high gain, ease of fabrication, and symmetric beam in the E- and H-planes, the antipodal Vivaldi antenna (AVA) is a promising solution for a variety of demanding tasks found in communication systems [1]. Owing to the antennas' flat design, they can easily be integrated with other microwave planar devices such as filters and mixers [2], [3]. While Vivaldi antennas theoretically have infinite bandwidth, their practical bandwidth is limited by a complex feeding network [4], [5]. In general, the antenna bandwidth is proportional to its length and aperture size; thus, when a greater bandwidth is required, the size of the antenna is increased. Miniaturization is another issue, where despite numerous AVA designs attempting to reduce their size, they invariably restrict the gain and stability of the radiation pattern [6], [7]. Numerous techniques exist for circumventing the gain limitations of conventional AVA, including using a Vivaldi array [8], a structure called a director in the tapered curved opening [9], and the use of metamaterial in front of the antenna as a load. An alternative technique entails inserting a metal director into the radiation flaring [10]. The use of arrays in specific applications has been large, complex, and costly. Additionally, PBGs are complicated in some ways. Furthermore, by utilizing "directors," energy is concentrated parallel to the antenna surface in two ways. First, using a dielectric with relative electric permittivity ε_r above the substrate is prohibitively expensive. Second, by loading both sides of the antenna substrate with an anisotropic zero-index slab [11], where this method adds complexity to the fabrication process while also increasing the directivity in the narrow bandwidth. The Substrate Integrated Waveguide (SIW) technology is suitable for microwave and millimeter frequency bands. The principle of this technology is to convert non-planar structures to planar structures. This technology has the advantages of both microstrip for easy integration in the same substrate as well as a conventional horn antenna for low losses. In addition, SIW structures can control surface wave trapping at higher frequencies [12], [13]. In recent years, there has been considerable interest in integrating various types of metamaterial unit cells with the tapered slot Vivaldi antenna (TSVA) to improve the overall radiation characteristics [14]. Zhou and Cui in [15] introduced metamaterials with zero refractive indexes (ZIM) in front of single- or multi-layer Vivaldi antennas to increase their directivity. The measurement results indicate that the Vivaldi antenna's directivity and efficiency have increased significantly in the designed ZIM bandwidth (9.5–10.5 GHz) but have remained stable in other frequency bands (2.5–9.5 GHz and 10.5–13.5 GHz). The authors in [16] introduced a single-layer and a multi-layer negative index metamaterial (NIM) to increase the antenna gain, where a modified ground plane for the proposed AVA was suggested and results compared to the conventional ground plane. The measurement results indicated an increase in gain between 9–20 GHz (the range in which

DOI: 10.13164/re.2022.0193

the refractive index is negative), with a maximum gain increase of 4 dBi, especially when a multi-layer metamaterial was used. The authors of [17] introduced a dual-slot Vivaldi antenna that was more directive than the traditional Vivaldi antenna. Kumar et al. in [18] sought to increase the antenna's directivity by incorporating a ZIM in front of the antenna presented in [17]. The antenna used in this paper operated between the frequencies of 2–10 GHz. By placing a metamaterial in front of the antenna as a load, the antenna's directivity increased by approximately 2 dBi.

In this paper, to increase the gain of the antipodal Vivaldi antenna fed by the substrate integrated waveguide structure, the phase of the radiation field must be uniform. This was accomplished by loading the antenna by using metamaterial with negative electric permittivity and negative magnetic permeability. The metamaterial structure is designed to compensate for phase and converts the spherical wave surface to a plane wave surface within a specified frequency range. The constructed structure had a higher gain than the non-metallic state, as determined by measurements. The measurements confirmed that the antenna has a wide bandwidth.

2. Metamaterial Unit Cell Design

It is necessary to design a structure that exhibits metamaterial properties within the antenna frequency band to maximize antenna efficiency. The fields applied to the unit cells must be aligned with the radiation fields of the Vivaldi antenna to achieve the desired response in the design of the metamaterial unit cell. This criterion is used to

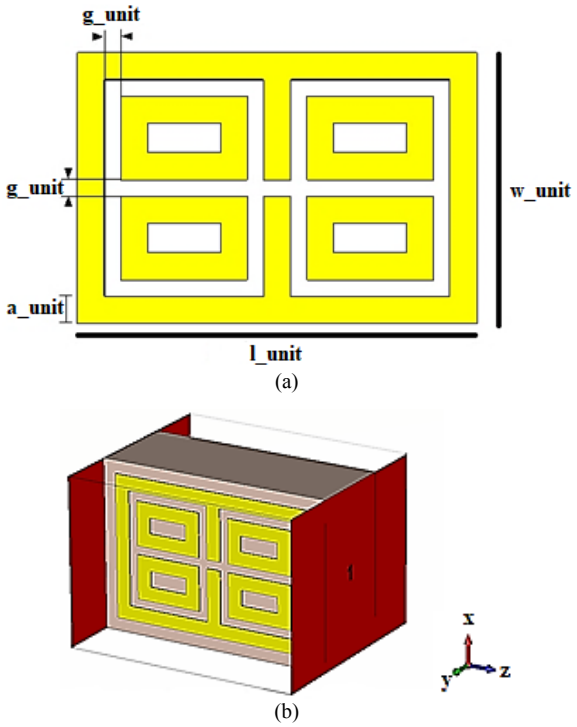

Fig. 1. (a) The structure of the metamaterial unit cell. (b) The simulated structure of the unit cell.

Parameter	l_unit	w_unit	a_unit	g_unit
Dimension (mm)	3.7	2.5	0.25	0.15

Tab. 1. Dimensions of the metamaterial unit cell.

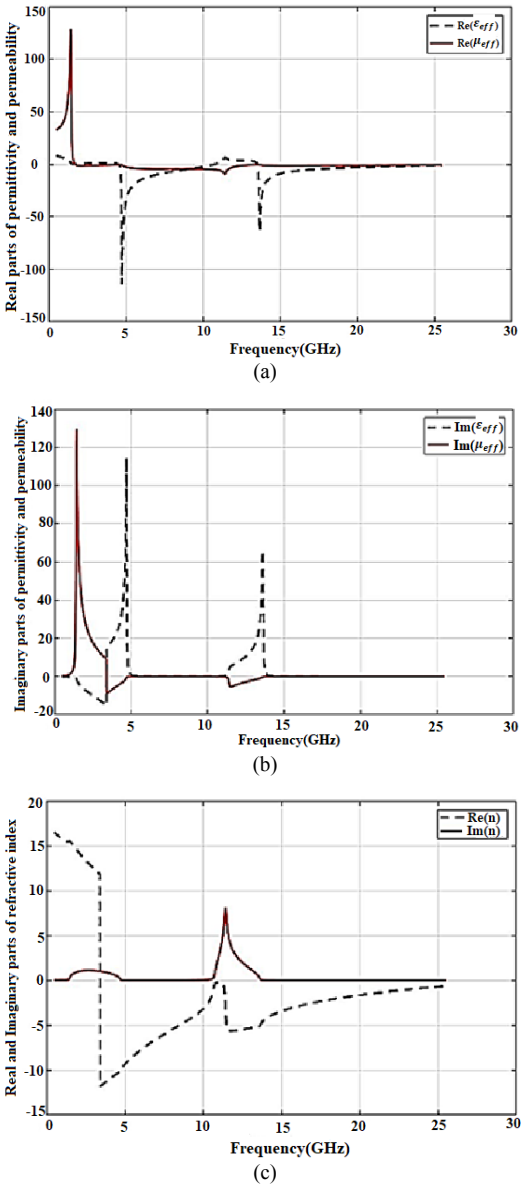

Fig. 2. The unit cell parameters are calculated using MATLAB: (a) The real parts of relative effective electric permittivity and magnetic permeability. (b) The imaginary parts of relative effective electric permittivity and magnetic permeability. (c) The unit cell refractive index.

determine the boundary conditions in the simulation of metamaterial unit cells. The electric field in the Vivaldi antenna is parallel to the antenna surface, while the magnetic field is perpendicular to the antenna surface. To accomplish this, perfect magnetic conductor (PMC) and perfect electric conductor (PEC) boundary conditions in a way that the electric field is parallel to the surface of the unit cell and the magnetic field perpendicular to the surface are placed. This unit cell is constructed to be easily loaded at the same height as the antenna.

Figure 1(a) shows the upper view of the designed metamaterial unit cell. Figure 1(b) illustrates the simulation setup for the unit cell in the CST studio. For two planes perpendicular to the x-axis, the boundary conditions are PEC; for two planes perpendicular to the y-axis, the boundary conditions are PMC. As illustrated in Fig. 1(b), the designed unit cell comprises a dielectric layer and a 0.018-mm-thick copper metallic layer. This structure is simulated on a substrate identical to the antenna (Rogers RT/duroid® 5880 with ε_r=2.2, loss tangent = 0.0009, and substrate thickness = 1.6 mm). The dimensions of the unit cell in the case of negatives ε and μ are listed in Tab. 1.

The values of effective relative permittivity and permeability and refractive index of metamaterial unit cell were calculated using the Smith method [19], MATLAB software, and the simulated scattering parameters. In terms of frequency, Figures 2(a) and 2(b) depict the real and imaginary parts of the effective relative permittivity and permeability, respectively and Figure 2(c) shows the unit cell refractive index. As can be seen from Fig. 2(b), the imaginary parts of the relative effective electric permittivity and magnetic permeability are nearly zero, indicating that the metamaterial structure has a negligible loss. Additionally, as illustrated in Fig. 2(a), the real parts of the relative effective electric permittivity and magnetic permeability are negative for frequencies greater than 5 GHz (except in the range of 10–13 GHz), confirming the metamaterial behavior of the designed unit cell.

3. Design of Vivaldi Antenna without SIW and Metamaterial

This research was inspired by the antipodal Vivaldi antenna presented in [20]. Specific parameters have been set to the values specified in these articles, while others, including the substrate's general specifications, have been modified to meet the antenna fabrication requirements.

3.1 Antenna Substrate

Choosing a suitable substrate is the first step in designing a microstrip antenna. One of the limitations in the design of a tapered slot antenna is its sensitivity to the substrate thickness. The dielectric constant, loss tangent and dielectric thickness of the substrate are all essential properties. The effective thickness of the substrate is obtained through (1) [21].

$$t_{\text{eff}} = t\left(\sqrt{\varepsilon_r} - 1\right) \tag{1}$$

where t denotes the substrate's physical thickness. When the effective thickness of the substrate is within the range specified in (2), the antenna performs satisfactorily.

$$0.005 \le \frac{t_{\text{eff}}}{\lambda_0} \le 0.03 \tag{2}$$

where λ_0 denotes the free-space wavelength. Due to fabrication constraints, the paper uses a Rogers RT/duroid® 5880 substrate with ε_r = 2.2, loss tangent of 0.0009, and a substrate thickness of 1.6 mm that meets the conditions of (2).

3.2 Antenna Width

Antenna width is another important parameter to consider when designing an antenna. The antenna width must exceed half the wavelength of the cut-off frequency. For optimal performance, the antenna's size should be at least half a wavelength. By decreasing this value, the low cut-off frequency is increased. In this paper, the antenna width is 12.6 mm, which is more than half the wavelength of the cut-off frequency.

3.3 Antenna Curve

The exponential functions of the antenna aperture located on the x-z plane and radiating in the z-axis direction are obtained from (3), (4), and (5):

$$x = c_1 \mathrm{e}^{az} + c_2, \tag{3}$$

$$c_1 = \frac{w_s + w_1}{2} \cdot \left(\mathrm{e}^{r \cdot l_{\text{ant}}} - 1\right)^{-1}, \tag{4}$$

$$c_2 = -\frac{w_s + w_1 \mathrm{e}^{r \cdot l_{\text{ant}}}}{2} \cdot \left(\mathrm{e}^{r \cdot l_{\text{ant}}} - 1\right)^{-1} \tag{5}$$

where r denotes the rate of tapering, l_{ant} denotes the aperture length, w_S represents the antenna width, and w_1 represents the overlap width. Figure 3 illustrates the antenna's structure, and Table 2 details the antenna's dimensions.

4. Antipodal Vivaldi Antenna Design Fed by SIW

The Vivaldi antenna is fed by SIW technology, which significantly reduces electric field leakage and enhances an-

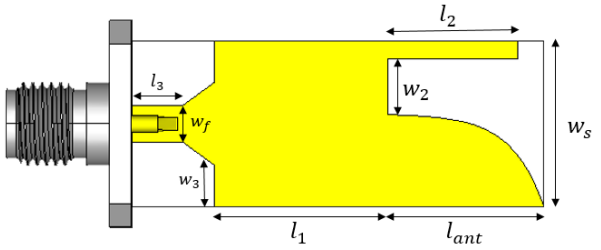

Fig. 3. Geometric structure of the antipodal Vivaldi antenna.

Parameter	l_{ant}	w_s	l_1	l_2	l_3
Dimension (mm)	11.9	12.6	13.3	9.9	3.9
Parameter	w_1	w_2	w_3	r	w_f
Dimension (mm)	1.4	4.2	3.2	0.4	2.8

Tab. 2. Antipodal Vivaldi antenna dimensions.

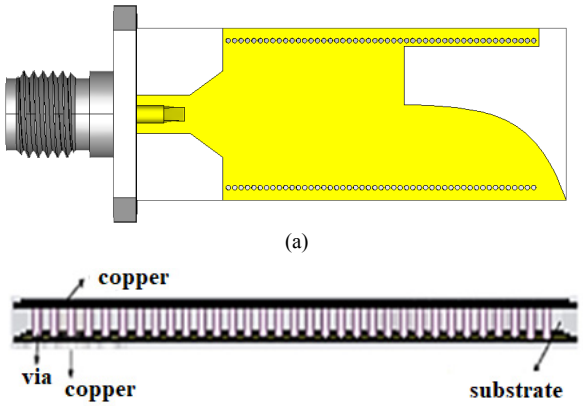

Fig. 4. Antipodal Vivaldi antenna structure fed by SIW: (a) Top view. (b) Side view.

tenna performance. In this paper, SIW technology to feed the Vivaldi antenna has been used. This part has been designed to enable the antenna to operate in TE_{10} mode. The diameter of the via (d) and the distance between the two vias (s) affect the reflection coefficient and antenna radiation, which must satisfy (6) and (7), respectively [22].

$$d < \frac{\lambda_g}{5}, \tag{6}$$

$$s \le 2d \tag{7}$$

where λ_g is the guided wavelength in the operating frequency.

In this study, d and s were considered to be 0.35 and 0.46 mm, respectively, fulfilling the above criteria. With the width of the SIW waveguide a, the cut-off frequencies of the TE_{10} and TE_{20} modes of the SIW structure can be calculated using (8) and (9) [23]

$$f_c(TE_{10}) = \frac{c}{2\sqrt{\varepsilon_r}}\left(a - \frac{d^2}{0.95 \times s}\right)^{-1}, \tag{8}$$

$$f_c(TE_{20}) = \frac{c}{\sqrt{\varepsilon_r}}\left(a - \frac{d^2}{1.1 \times s} - \frac{d^3}{6.6s^2}\right)^{-1}. \tag{9}$$

When a = 10.75 mm, the TE_{10} and TE_{20} modes have cut-off frequencies of 9.6 GHz and 21 GHz, respectively (SIW width determines the cut-off frequency and propagation constant in the first mode). The structure of the antipodal Vivaldi antenna fed by SIW is depicted in Fig. 4.

When a microstrip structure feeds an antenna, the wave is reflected by hitting the top and bottom planes and exiting through the sidewalls due to the openness of the microstrip walls. As a result, solely microstrip feeding increases the sidelobe level (SLL) and decreases the antenna's gain. By selecting the SIW feeding, the leakage wave is reduced, and the overall performance of the antenna is improved. The reflection coefficients for an antenna fed via microstrip and an antenna fed via microstrip to SIW transition are shown in Fig. 5. As shown in this figure, there is

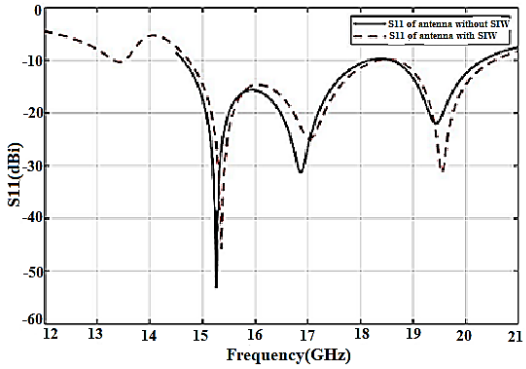

Fig. 5. The reflection coefficients of the antenna with conventional microstrip feeding and with SIW feeding.

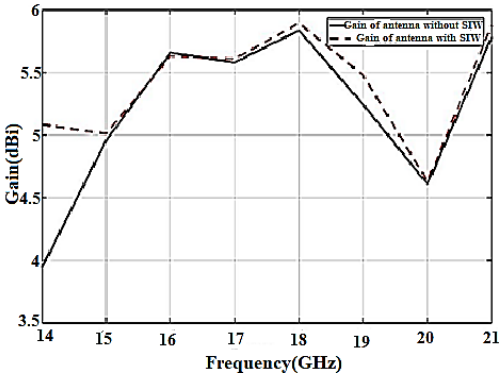

Fig. 6. The gain of conventional antenna and gain of SIW fed antenna.

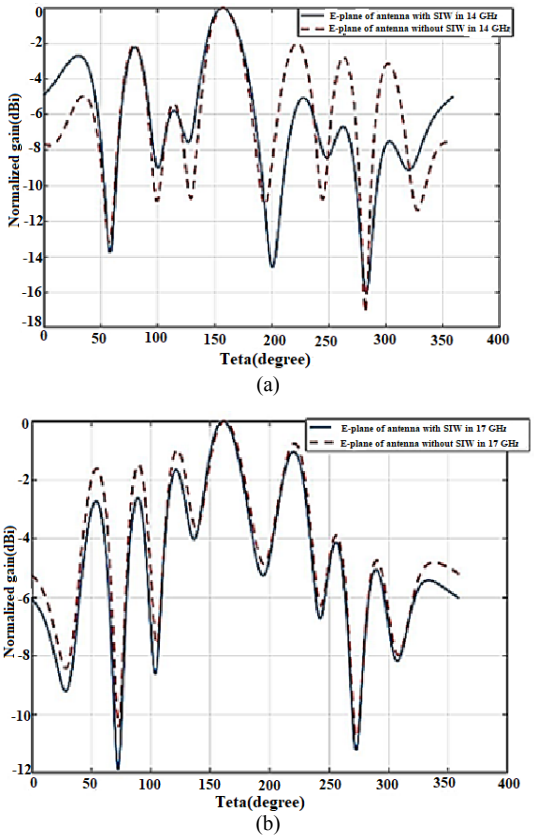

Fig. 7. Normalized radiation patterns of the antenna with and without SIW feed at: (a) 14 GHz, (b) 17 GHz.

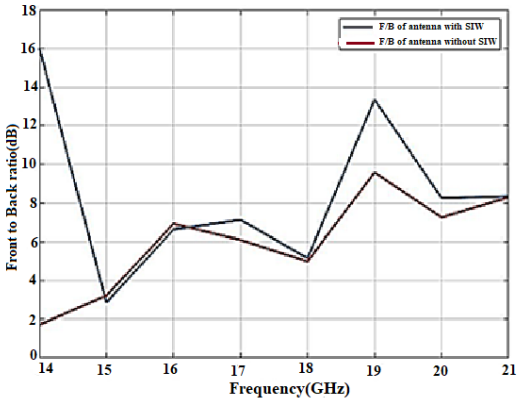

Fig. 8. FBR of the antenna without SIW feed and with SIW feed.

a negligible frequency shift when the SIW is used (approximately 0.2 GHz) which is very desirable. Figure 6 depicts the antenna's gain with and without SIW. As displayed in Fig. 6, the SIW feeding increases the antenna's gain (which is relatively insignificant to about 1.2 dBi).

The normalized gain in terms of spatial angle on the E-plane is shown in Figs. 7(a) and 7(b) at 14 GHz and 17 GHz and for two states with and without SIW. These plots confirm the reduction in sidelobe level at these frequencies. The front-to-back ratio (FBR) is also shown in Fig. 8, demonstrating the antenna's superior performance with SIW feed, because it reduces wave leakage.

5. Antipodal Vivaldi Antenna Loaded with Metamaterial Unit Cell

Figure 9 shows the structure of an antipodal Vivaldi antenna loaded with a metamaterial unit cell.

This structure comprises 21 metamaterial unit cells that are identical in height to the antenna and are mounted on the same substrate. Figure 10 compares the $|S_{11}|$ of the antenna with metamaterial array to the $|S_{11}|$ of the antenna without it. As depicted in Fig. 10, the $|S_{11}|$ of antenna is less than –10 dB in the frequency range of 14.7–20.5 GHz and has remained constant compared to the antenna's bandwidth without the metamaterial. Furthermore, Figure 11 illustrates an increase in antenna efficiency following the metamaterial loading. As shown in Fig. 11, the gain of the loaded antenna has increased to about 2.1 dBi. Metamaterial unit cells act as field concentrators, thereby increasing the gain. Additionally, this structure reduces the substrate's electric permittivity due to its properties. This reduces dielectric loss and thus increases the structure's efficiency.

The phase distribution of the electric field becomes more uniform when the antenna is loaded with the metamaterial array because metamaterial unit cells act as field concentrators, thereby spherical phase fronts become planes. This phenomenon is shown in Figs. 12(a)–(f) at 14, 16, and 20 GHz.

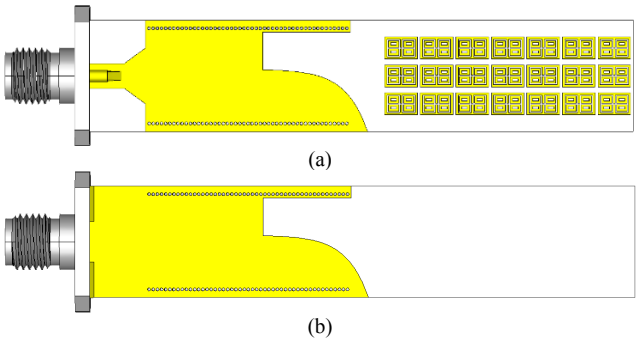

Fig. 9. Antipodal Vivaldi antenna structure loaded with metamaterial unit cell: (a) top view, (b) bottom view.

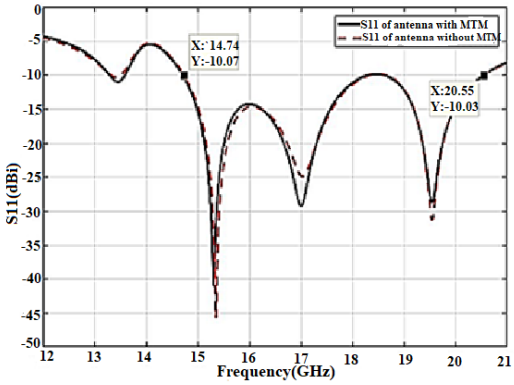

Fig. 10. $|S_{11}|$ of the antenna in the presence of metamaterial and without the metamaterial array.

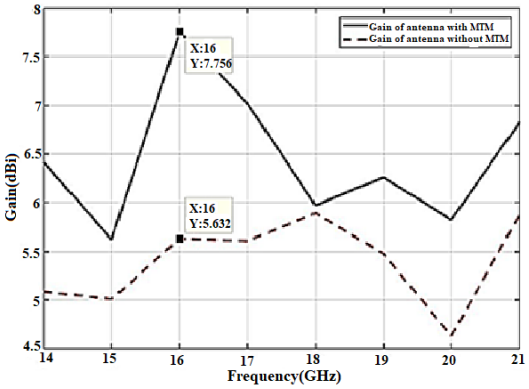

Fig. 11. Antenna gain in the presence of metamaterial and without the metamaterial array.

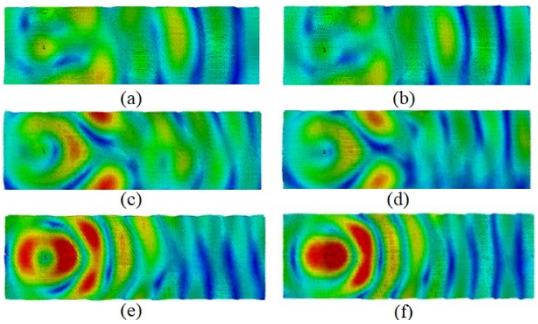

Fig. 12. Electric field distribution of the antenna in the absence of metamaterial at (a) 14 GHz, (c) 16 GHz, and (e) 20 GHz. Electric field distribution of the antenna in the presence of metamaterial at (b) 14 GHz, (d) 16 GHz, and (f) 20 GHz.

The co-polarization components in the E-plane radiation pattern, for unloaded and loaded antenna, at frequencies 14, 16 and 20 GHz, are shown in Figs. 13(a)–(c). As mentioned earlier, metamaterials act as a centralizing structure and thus the loaded antenna has a more direct radiation pattern, as can be seen from these figures. Also, Figures 14(a)–(c) show the antenna's normalized gain at 14,

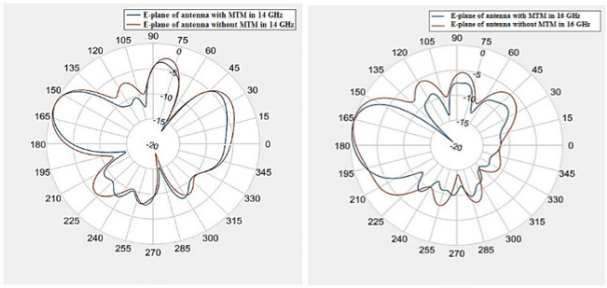

(a) (b)

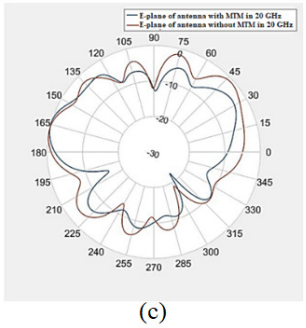

(c)

Fig. 13. The E-plane radiation patterns of the antenna with and without metamaterial array, at (a) 14 GHz, (b) 16 GHz, and (c) 20 GHz.

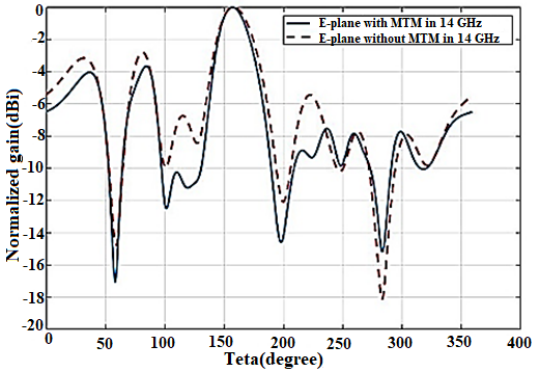

(a)

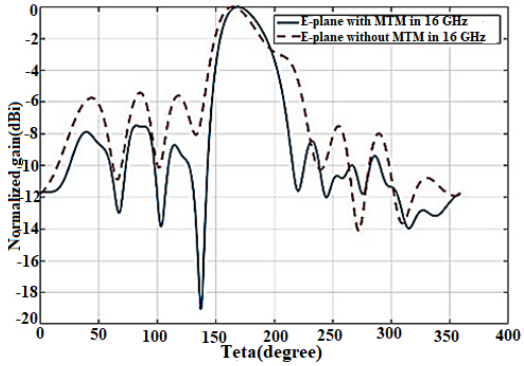

(b)

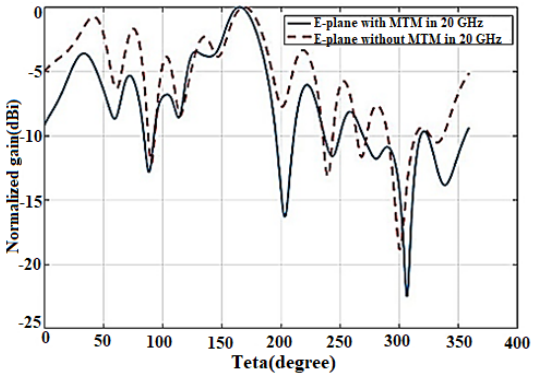

(c)

Fig. 14. The E-plane normalized gain of the antenna in terms of spatial angle with and without metamaterial array, at (a) 14 GHz, (b) 16 GHz, and (c) 20 GHz.

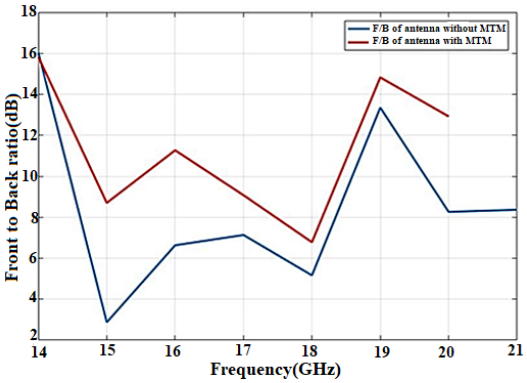

Fig. 15. The FBR of the antenna with and without metamaterial.

16, and 20 GHz in terms of spatial angle in the E-plane. The figures indicate that the sidelobe level has also been numerously modified. Figure 15 depicts the antenna's FBR ratio with and without the metamaterial array. By placing the metamaterial and concentrating the radiated waves from the antenna, its gain increases and FBR also increases. Given the small size of the structure presented in this paper, this increase in FBR is an important advantage.

6. The Fabricated Antenna

The structure of the final design is shown in Fig. 16. To feeding of the antenna, the SMA 6551F1 connector is used. After reviewing the simulation results, the antenna loaded with metamaterial unit cells was built and tested in the antenna room. The reflection coefficient, the antenna radiation pattern, and its efficiency were measured in the anechoic chamber. It should be noted that only the frequency range of 12–18 GHz was measured due to several constraints.

(a) (b)

Fig. 16. Fabricated antenna: (a) top view, (b) side view.

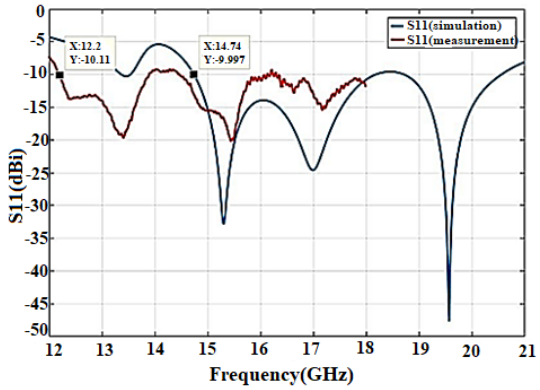

Fig. 17. Reflection coefficient results from simulation and measurement.

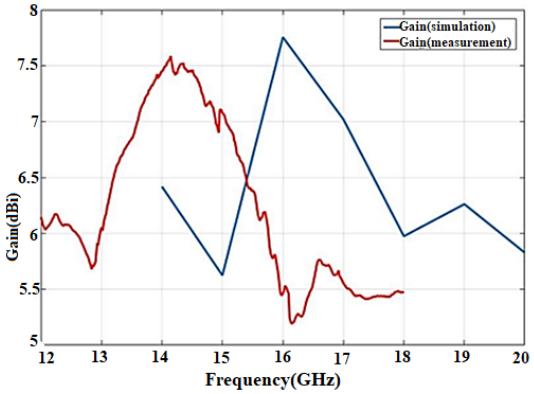

Fig. 18. Comparison of antenna simulation and measurement gain results.

The $|S_{11}|$ values obtained through measurement and simulation follow a nearly identical trend. The difference is that the measurement results exhibit a 2.5 GHz frequency shift, which could result from fabrication accuracy or the antenna room's lack of isolation. These findings are depicted in Fig. 17. Finally, in Fig. 18, the antenna simulation and measured gain were compared. The frequency shift visible in the reflection coefficient plot is also visible here.

7. Conclusions

This research investigates an antipodal Vivaldi antenna equipped with SIW technology at a frequency range of 14.7–20.5 GHz. In general, it is challenging to achieve high efficiency with Vivaldi antennas due to the antenna's radiation aperture being constrained by the low height of the dielectric substrate. SIW feeding and metamaterial structure, respectively, are proposed as methods in this paper for achieving lower losses and increased efficiency. Alternately, the metamaterial structure was used as a load in front of the antenna. The metamaterial proposed in this paper had minimal losses and could operate over a wide frequency range. Additionally, the SIW was designed to operate in TE_{10} mode, where the antenna and metamaterial structure was simulated and optimized using CST, and the unit cell effective parameters were extracted using MATLAB.

Acknowledgment

The authors consider it necessary to express their sincere gratitude to Iran Madar Sanat Company.

References

[1] HOOD, A. Z., KARACOLAK, T., TOPSAKAL, E. A small antipodal Vivaldi antenna for ultrawide-band applications. *IEEE Antennas and Wireless Propagation Letters,* 2008, vol. 7, p. 656–660. DOI: 10.1109/LAWP.2008.921352

[2] GJOKAJ, V., PAPAPOLYMEROU, J., ALBRECHT, J. D., et al. A compact receive module in 3-D printed Vivaldi antenna. *IEEE Transactions on Components, Packaging and Manufacturing Technology,* 2019, vol. 10, no. 2, p. 343–346. DOI: 10.1109/TCPMT.2019.2961345

[3] YANG, K., HOANG, M. H., BAO, X., et al. Dual-stub Ka-band Vivaldi antenna with integrated bandpass filter. *IET Microwaves, Antennas & Propagation,* 2018, vol. 12, no. 5, p. 668–671. DOI: 10.1049/iet-map.2017.0488

[4] GIBSON, P. The Vivaldi aerial. In *The 9th European Microwave Conference*. Brighton (UK), 1979, p. 101–105. DOI: 10.1109/EUMA.1979.332681

[5] JANASWAMY, R., SCHAUBERT, D. Analysis of the tapered slot antenna. *IEEE Transactions on Antennas and Propagation,* 1987, vol. 35, no. 9, p. 1058–1065. DOI: 10.1109/TAP.1987.1144218

[6] BAI, J., SHI, S., PRATHER, D. W. Modified compact antipodal Vivaldi antenna for 4–50-GHz UWB application. *IEEE Transactions on Microwave Theory and Techniques,* 2011, vol. 59, no. 4, p. 1051–1057. DOI: 10.1109/TMTT.2011.2113970

[7] FEI, P., JIAO, Y. C., HU, W., et al. A miniaturized antipodal Vivaldi antenna with improved radiation characteristics. *IEEE Antennas and Wireless Propagation Letters,* 2011, vol. 10, p. 127–130. DOI: 10.1109/LAWP.2011.2112329

[8] OMAR, S. A., IQBAL, A., SARAEREH, O. A., et al. An array of M-shaped Vivaldi antennas for UWB applications. *Progress in Electromagnetics Research Letters,* 2017, vol. 68, p. 67–72. DOI: 10.2528/PIERL17041506

[9] LIU, H., YANG, W., ZHANG, A., et al. A miniaturized gain-enhanced antipodal Vivaldi antenna and its array for 5G communication applications. *IEEE Access,* 2018, vol. 6, p. 76282–76288. DOI: 10.1109/ACCESS.2018.2882914

[10] LI, L., XIA, X., LIU, Y., et al. Wideband balanced antipodal Vivaldi antenna with enhanced radiation parameters. *Progress in Electromagnetics Research,* 2016. vol. 66, p. 163–171. DOI: 10.2528/PIERC16051704

[11] ELSHERBINI, A., ZHANG. C., LIN. S., et al. UWB antipodal Vivaldi antennas with protruded dielectric rods for higher gain, symmetric patterns and minimal phase center variations. In *2007 IEEE Antennas and Propagation Society International Symposium*. Honolulu (USA), 2007, p. 1973–1976. DOI: 10.1109/APS.2007.4395909

[12] SELLAL, K. On substrate integrated waveguide slot antennas. *Microwave and Optical Technology Letters,* 2015, vol. 57, no. 6, p. 1511–1516. DOI: 10.1002/mop.29125

[13] OKAN, T., AKCAM, N. Wideband low-cost FR4 epoxy-based antenna with H-shaped slot for V-band applications. *International Journal of RF and Microwave Computer-Aided Engineering,* 2021, vol. 31, no. 2, p. 1–9. DOI: 10.1002/mmce.22348

[14] BHASKAR, M., JOHARI, E., AKHTER, Z., et al. Gain enhancement of the Vivaldi antenna with band notch characteristics using zero-index metamaterial. *Microwave and Optical Technology Letters,* 2016, vol. 58, no. 1, p. 233–238. DOI: 10.1002/mop.29534

[15] ZHOU, B., CUI, T. J. Directivity enhancement to Vivaldi antennas using compactly anisotropic zero-index metamaterials. *IEEE Antennas and Wireless Propagation Letters,* 2011, vol. 10, p. 326–329. DOI: 10.1109/LAWP.2011.2142170

[16] ALHAVARI, A. R. H., ISMAIL, A., MAHDI, M. A., et al. Antipodal Vivaldi antenna performance booster exploiting snug-in negative index metamaterial. *Progress in Electromagnetics Research,* 2012, vol. 27, p. 265–279. DOI: 10.2528/PIERC12012906

[17] WANG, Y. W., WANG, G. M., ZONG, B. F. Directivity improvement of Vivaldi antenna using double-slot structure. *IEEE Antennas and Wireless Propagation Letters,* 2013. vol. 12, p. 1380–1383. DOI: 10.1109/LAWP.2013.2285182

[18] KUMAR, P., AKHTER, Z., JHA, A. K., et al. Directivity enhancement of double slot Vivaldi antenna using anisotropic zero-index metamaterials. In *IEEE International Symposium on Antennas and Propagation & USNC/URSI National Radio Science Meeting*. Vancouver (Canada), 2015, p. 2333–2334. DOI: 10.1109/APS.2015.7305555

[19] SMITH, D., VIER, D., KOSCHNY, T., et al. Electromagnetic parameter retrieval from inhomogeneous metamaterials. *Physical Review E,* 2005, vol. 71, no. 3, p. 1–11. DOI: 10.1103/PhysRevE.71.036617

[20] KAZEMI, R., FATHY, E., SADEGHZADEH, R. A. Ultra-wide band Vivaldi antenna array using low loss SIW power divider and GCPW wide band transition. In *2012 IEEE Radio and Wireless Symposium*. Santa Clara (USA), 2012, p. 39–42. DOI: 10.1109/RWS.2012.6175309

[21] MAHDAVI. D., SUDHAKAR. A. Design and development of tapered slot Vivaldi antenna for ultra-wideband applications. *IAETSD Journal for Advanced Research in Applied Sciences,* 2018, vol. 5, no. 4, p. 511–515. ISSN: 2394-8442

[22] NAWAZ, M. I., HUILING, Z., KASHIF, M. Substrate integrated waveguide (SIW) to microstrip transition at X-band. In *Proceedings of the 2014 International Conference on Circuits, Systems and Control*. Interlaken (Switzerland), 2014, p. 61–63. ISBN: 978-1-61804-216-3

[23] CASSIVI, Y., PERREGRINI, L., ARCIONI, P., et al. Dispersion characteristics of substrate integrated rectangular waveguide. *IEEE Microwave and Wireless Components Letters,* 2002, vol. 12, no. 9, p. 333–335. DOI: 10.1109/LMWC.2002.803188

About the Authors ...

Arman BORDBAR was born in Bandarelengeh, Iran, in 1989. He received the BS degree in Communication Engineering from Shahrekord University in 2014 and MS degree in Communication Engineering from Shiraz University in 2017. His research interests include theoretical and computational electromagnetics and antenna design.

Farzad MOHAJERI (corresponding author) was born in Shiraz, Iran, in 1967 and is an Associate Professor in Communications Department, Shiraz University. He received the BS degree in Electronics Engineering and MS degree in Communication Engineering from Shiraz University in 1991 and 1994, respectively, and Ph.D. degree in Communication Engineering from Tarbiat-Modarres University in 2001. His research interests include computational electromagnetics and antenna design.

Zahra GHORBANI was born in Fasa, Iran, in 1995. She received the BS degree in Communication Engineering from Shahid Bahonar, Kerman University in 2017 and MS degree in Communication Engineering from Shiraz University in 2019. Her research interests include antenna theory and design.